INORGANIC CHEMISTRY
FRONTIERS

RESEARCH ARTICLE

View Article Online
View Journal | View Issue

Cite this: *Inorg. Chem. Front.*, 2026, **13**, 4084

[2 + 2] Photocycloaddition induces a 114 K high-temperature shift of the spin-crossover transition: the role of cycloaddition-induced strain

Marcin Kaźmierczak,*[a] Vladyslav Maliuzhenko,[a] Aleksandra Tołoczko,[a] Marek Weselski,[a] Miłosz Siczek,[a] Juliusz A. Wolny,[b] Volker Schünemann[b] and Robert Bronisz*[a]

Herein, 6-(1,2,3-triazol-1-ylmethyl)coumarin (**L1**), which can combine molecule photoreactivity and spin-crossover activity in Fe(II) complexes, was prepared by reacting 6-(bromomethyl)coumarin with sodium salt 1,2,3-triazole. **L1** forms mononuclear systems $[Fe(\mathbf{L1})_6](ClO_4)_2{\cdot}n CH_3CN$ (n = 0, 2). The solvated form (**1**) exhibits complete, one-step spin-crossover at $T_{1/2}$ = 155 K. In **1**, there is a competition between two coumarin fragments from two ligand molecules for access to a third fragment located between them. The distances between the double bonds of the lactone rings are equal to 3.70 and 3.92 Å, and light irradiation at a wavelength of 365 nm results in [2 + 2] cycloaddition. Although photoconversion can proceed in two directions, this competition ultimately yields a two-dimensional polymer layer with a frustrated topology. The resulting complex (**1c**) also exhibits spin crossover, showing a slight shift to lower temperatures ($T_{1/2}$ = 141 K). The non-solvated complex (**2**) exhibits a two-step spin-crossover ($T^1_{1/2}$ = 83 K and $T^2_{1/2}$ = 62 K). In contrast to **1**, only one type of ligand pair exists for which topochemical requirements are fulfilled. In effect, a regular (2,2) polymeric layer is formed as a result of the [2 + 2] photocycloaddition (λ = 365 nm). This results in an unprecedented shift in the spin crossover to higher temperatures up to 197 K. The photoconversion product (**2c**) is characterized by the presence of strong strains involving dimerized ligand molecules, particularly cyclobutane rings. DFT modelling based on the structure of the dimerized ligand reveals a significant difference in this strain, and the energetic effect of it (stress) is more than 240 kJ mol^{-1} higher for the ligands corresponding to the complex in the HS state. This is consistent with the observed 114 K shift of the transition temperature upon transformation from the initial mononuclear complex to the photoconverted 2D structure.

Received 14th November 2025,
Accepted 7th March 2026

DOI: 10.1039/d5qi02305j

rsc.li/frontiers-inorganic

Introduction

Research on light-induced phenomena,[1] including structural transformations, is a dynamically developing study area.[2] A group of compounds constituting a promising platform for modulating properties as a result of photoconversion are systems exhibiting the spin crossover (SCO) phenomenon.[3,4] The electronic structure of such compounds based on $3d^4$–$3d^7$ transition-metal ions is very sensitive to the environment, both to the type of chromophore[5] and, importantly, to the occurrence of structural transformations.[6] This fact is reflected in the occurrence of non-conventional transitions, such as two-channel spin-crossover,[7] multiway spin-crossover,[8] reverse spin-crossover[9] and combinations of normal and reverse spin-crossover.[10] These examples illustrate the feasibility of complex sequences of disturbance-response processes and provide an excellent justification for the advisability of introducing photoresponsive fragments into the molecules of spin-crossover systems.

Studies of azopyridine-based coordination compounds revealed that *cis*/*trans* photoisomerization is possible and causes spin-state switching (LD-LISC),[11] but these processes take place noticeably in solution, in the form of a dispersion in the cellulose acetate matrix[12] as well as in thin films.[13,14] An application of 2,6-di(1*H*-pyrazol-1-yl)-4-styrylpyridine by Nishihara succeeded in one-way switching in solid.[15] An extension of the concept of using molecules undergoing intramolecular isomerization was the use of bis(thienyl)ethene-type fragments. Additionally, in this case, successfully performed photoisomerization affected spin-crossover behavior.[16–19] A different approach is the use of photoinduced, intermolecular

[a]*Faculty of Chemistry, University of Wrocław, F. Joliot-Curie 14, 50-383 Wrocław, Poland. E-mail: robert.bronisz@uwr.edu.pl*
[b]*Faculty of Physics, RPTU Kaiserslautern-Landau, Erwin Schrödinger Str., 46 67663 Kaiserlautern, Germany*

[2 + 2] cyclization. However, the number of systems of this type is very limited. In this approach, ligand molecules, guest molecules,[20] and counterions[21] are used. The use of styrylpyridine (spy) or *trans*-1-(2-pyridyl)-2-(4-pyridyl)ethylene (2,4-bpe) resulted in a shift in the spin crossover to lower temperatures, a decrease in cooperativity combined with incomplete spin-crossover, or even the loss of the ability to thermally induce spin crossover.[22,23]

Such an extremely small number of implementations indicates low effectiveness in meeting the topochemical conditions, which directly results from the unpredictability of the crystal structures of novel coordination compounds. To overcome this barrier, we have recently exploited as a photoreactive unit 7-(tetrazol-2-ylmethyl)coumarin (**L**, Scheme 1), which contains a flat photoreactive coumarin fragment and readily forms layered structures required to satisfy the topochemical requirements in the solid state. In the case of mononuclear system $[Fe(\mathbf{L})_6](BF_4)_2{\cdot}4CH_3CN$, the 0 D → 1 D structural conversion entailed a transition from a system exhibiting thermally induced complete spin crossover to a coordination polymer remaining in a high-spin state down to 10 K.[24] Such a decisive change in the spin-crossover properties of systems undergoing intermolecular [2 + 2] cyclization became an incentive to gain deeper insight into both the structural processes related to photoconversion and their influence on the spin state. Continuing this research, we decided to maintain the general scheme of the ligand molecule structure, in which the methylene linker connecting the coumarin fragment with the donor group is responsible for the adaptation of the ligand shape with respect to neighboring molecules, thus facilitating the fulfillment of the topochemical requirements.[25–28]

In this study, we used a new photoreactive ligand system by replacing the tetrazol-2-yl group with a 1,2,3-triazole ring and changing the donor anchoring site in the coumarin fragment (Scheme 1). We present the structural consequences of photoconversion processes (i) occurring between unambiguously defined, which are topochemically favored pairs of coumarin fragments, and (ii) depending on the unique competition between two topochemically favored coumarin-based pairs. The resulting structural conversions affected spin-crossover properties, in particular leading to the first observation of an extremely strong shift of the spin crossover towards higher temperatures.

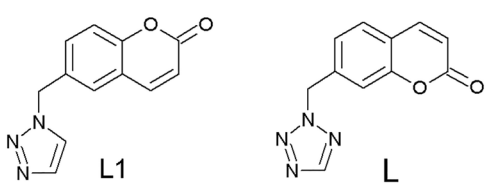

Scheme 1 Structures of 6-(1,2,3-triazol-1-ylmethyl)coumarin (**L1**) and 7-(tetrazol-2-ylmethyl)coumarin (**L**).

Results and discussion

Ligands and complexes: general characterization

Recently, we presented the preparation of 7-(tetrazol-2-ylmethyl)coumarin (**L**) depending on the alkylation of tetrazole with 7-(bromomethyl)coumarin. The novel 1,2,3-triazole-based ligand 6-(1,2,3-triazol-1-ylmethyl)coumarin (**L1**, Scheme 1) used in these studies was obtained analogously by reacting 6-(bromomethyl)coumarin with the sodium salt of 1,2,3-triazole (see SI for synthetic details). **L1** was isolated as a colorless crystal with a yield of 21%. The synthesis yield results from the lack of regioselectivity in the alkylation reaction of 1*H*-1,2,3-triazole (see SI).

Depending on the conditions, reactions between **L1** and iron(II) perchlorate (molar ratio: 6 : 1) carried out in acetonitrile can lead to the formation of two compounds. The formation of very thin, colorless plates of $[Fe(\mathbf{L1})_6](ClO_4)_2{\cdot}2CH_3CN$ (**1**) starts within 2–3 days after combining the reagents. If the crystalline product is left in the mother liquor for 3 weeks, a single-crystal-to-single-crystal transformation begins. The formation of colorless blocks of novel compound $[Fe(\mathbf{L1})_6](ClO_4)_2$ (**2**) is very slow (months). It is worth noting that seeding the reaction mixture with crystals of previously prepared compound **2** leads to the growth of the crystalline product within 2–3 weeks.

The complexes are stable during storage in a nitrogen atmosphere. Importantly, cooling colorless crystals of **1** and **2** in liquid nitrogen results in the appearance of a violet color, which indicates the occurrence of the $^5T \rightarrow {}^1A$ spin-crossover.

Spin-crossover properties of $[Fe(L1)_6](ClO_4)_2{\cdot}2CH_3CN$ (1)

The primary sample of **1** remains at room temperature in a high spin (HS) form. During cooling, the value of $\chi_M T$ = 3.4 cm^3 K mol^{-1} remains practically unchanged down to 220 K. Further cooling is accompanied by quite an abrupt reduction of $\chi_M T$, which indicates thermally induced spin-crossover (Fig. 1). Complete spin-crossover with $T_{1/2}$ = 155 K is achieved at about 120 K. The $\chi_M T(T)$ dependence recorded in the heating mode is practically the same as that recorded during cooling.

Mössbauer spectrum of **1** at 260 K (Fig. S3) is composed of one quadrupole doublet (ΔE_Q = 1.31 mm s^{-1}, δ = 1.04 mm s^{-1}), indicating the homogeneity of the sample. A decrease in temperature is accompanied by the appearance of the LS component. Lowering the temperature results in the vanishing of the HS form, and at 140 K (Fig. S3c), only the LS form (ΔE_Q = 0.32 mm s^{-1}, δ = 0.53 mm s^{-1}) is observed. The temperature dependence of the relative area of the HS form derived from ($A_{HS}/(A_{HS} + A_{LS})$) very well corresponds to the results of the magnetic studies (Fig. S4), which confirms the homogeneity of the sample.

In **1**, there is one crystallographically independent Fe(II) ion in the crystal lattice. The first coordination sphere of Fe(II) consists of six 1,2,3-triazole rings linked through *exo*-located nitrogen atoms N3 (Fig. 2a, Fig. S1). At 250 K, the Fe–N distances are equal to 2.176(2), 2.178(2) and 2.246(2) Å. The N–Fe–N angles are in the range of 87.9(1)°–92.2(1)° (Σ = 14.1°). Cooling

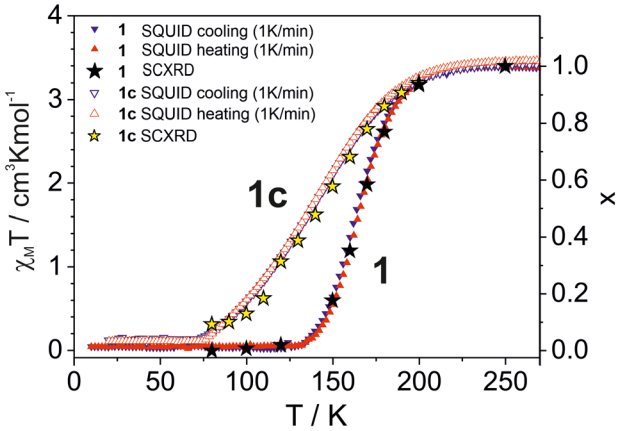

Fig. 1 Temperature dependences of $\chi_M T$ (SQUID) and relative areas of the HS form derived from single-crystal X-ray diffraction studies for **1** and **1c**. x is defined for SCXRD as $(d^{T}_{Fe-N} - d^{LS}_{Fe-N})/(d^{HS}_{Fe-N} - d^{LS}_{Fe-N})$, where d is the average Fe–N distance determined at temperature T for HS and LS forms. d^{LS}_{Fe-N} is estimated considering that at 80 K, the contribution of the HS form equals 0.05 according to Mössbauer spectroscopy (SI).

the crystal to 80 K results in shortening of Fe–N distances to 1.984(2), 1.987(2) and 2.023(2) Å. These values are close to those expected for complete spin-crossover. The N–Fe–N angles adopt values in the range of 88.5(1)°–91.7(1)°, and a slight reduction in the distortion of the FeN_6 chromophore as a result of the formation of an LS form occurs (Σ = 9.1°). Spin crossover does not involve other serious structural changes, such as coordinated ligand molecules, anions and acetonitrile molecules.

Photoconversion studies 1 → 1c

In **1**, one pair of ligand molecules is directed into the Fe(II) ion along [010] and the second one is directed into the [0–10] direction (Fig. 2a). This results in the formation of columns in which iron atoms are separated by a distance of 11.3 Å (250 K). The coumarin fragments arising from neighboring Fe(II) ions arranged along the *b* direction (blue- and yellow-colored molecules in Fig. 2a) are parallel to each other. Nevertheless, they are twisted at *ca.* 43° (Fig. S2). Distances between the centers of the double bonds of lactone rings are equal to *ca.* 3.92 Å (red dotted lines in Fig. 2a). The remaining two coumarin fragments are directed along the *c* direction into two neighboring columns (Fig. S2). Coumarin fragments from neighboring columns are arranged parallel to each other, and the distance between the centers of the double bonds of lactone rings is equal to 3.70 Å (black dotted lines on Fig. 2a). Additionally, here, coumarin fragments are twisted with respect to each other at *ca.* 30°. In this way, a layered, supramolecular structure is formed in which coumarin fragments are oriented head-to-head in two directions.

FTIR microscopy. Initially, the ability to induce photocyclization in **1** was tested using FTIR microscopy measurements. Irradiation (365 nm, 293 K, 1 W) of a very thin plate resulted

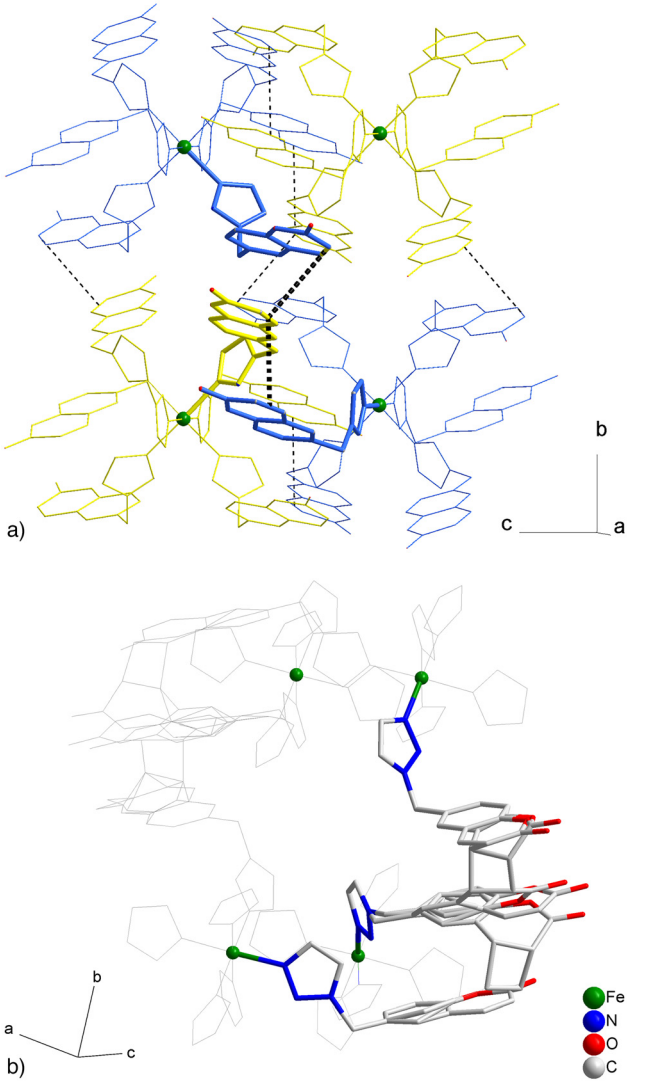

Fig. 2 Coumarin fragments in **1** fulfilling topochemical conditions, originating from $[FeL_6]^{2+}$ cations (marked in blue and yellow for better readability) arranged along the *b* direction, are linked with the red dotted lines, while those arranged along *c* direction are joined with black dotted lines (a). Structure of the photocyclization product **1c**, showing the competition between coumarin fragments (thick lines) arranged along the *b* and *c* directions (b).

in the appearance of new peaks at 1150 and 1206 cm^{-1}, accompanied by a general increase in the intensity across the 1150–1300 cm^{-1} range (Fig. 3a). Based on DFT studies, these changes can be attributed to δ(C–H) bending vibrations arising from the formation of a cyclobutane ring. The changes also include carbonyl group vibrations ν(C=O). A new band, which shifts toward higher frequencies, appears. It should be noted that the changes are less pronounced than those in the previously reported system $[Fe(\mathbf{L})_6](BF_4)_2{\cdot}4CH_3CN$.[24] Notably, photoconversion does not affect the ν(CN) vibration of the acetonitrile molecule. It was established that exposure longer than 120 s did not lead to further changes in the spectrum.

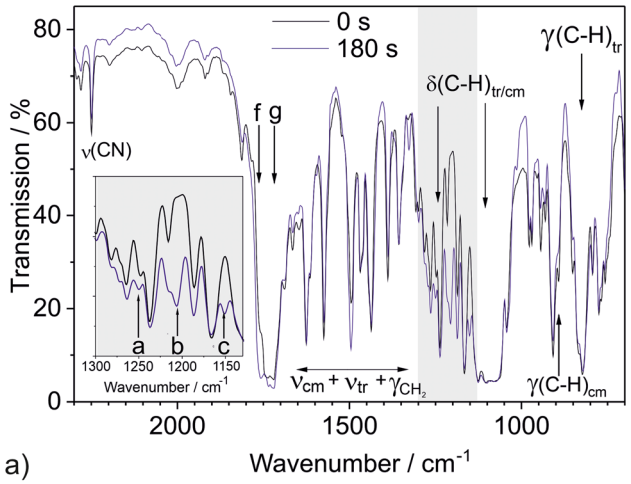

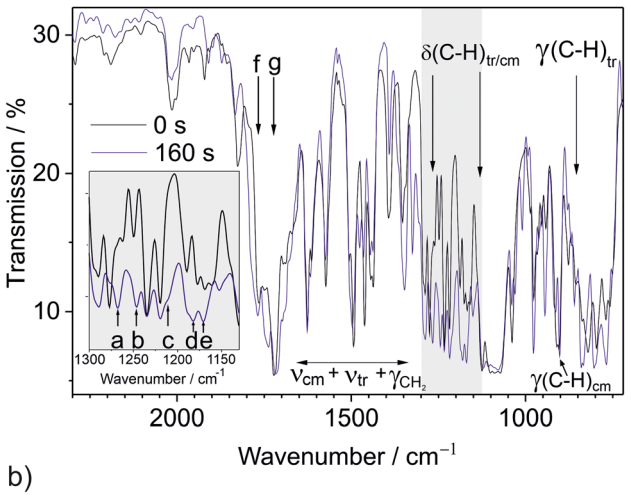

Fig. 3 FTIR microscopy spectra recorded before and after illumination of crystals **1** (a) and **2** (b) with light of wavelength 365 nm (1 W). For **1**, the band assignment is based on DFT results (see SI for details). The letters denote the peaks that either appear (a–c) or show an increase (d and e). Peak a–c may be assigned to the vibrations of the cyclobutane ring. They are predicted to occur at 1244 cm^{-1}, 1208 and 1172 cm^{-1} and correspond to the modes involving cyclobutane C–H bending coupled with coumarin (cm) in-plane C–H bending (see the movies in SI). In the case of carbonyl stretching, the changes may be related to a predicted shift in the lactone stretching with the calculated mode at a higher energy occurring at *ca.* 1778 cm^{-1}, compared to that at 1760 cm^{-1} found for the coumarin ligand in mononuclear **2** (see movies in SI). The latter effect is more clearly observed in the powder spectra of **1**, **1c**, **2** and **2c** in Nujol (see SI). For **1**, the main peak at 1749 cm^{-1} shifts to 1770 cm^{-1} upon conversion, while for **2**, a corresponding shift from 1730 (peak f) to 1756 cm^{-1} (peak g) is observed. Notably, for the process of photoconversion of **2**, 5 new peaks in the area of cyclobutane C–H bending may be identified (denoted a–e). "tr" denotes 1,2,3-triazole. The inset shows a range of 1300–1120 cm^{-1} (marked with a grey background). Finally, it is noteworthy that for both **1** and **2**, the IR spectra in Nujol reveal the appearance of a new peak at *ca.* 760 cm^{-1} in the photoconverted complex. DFT modelling indicates that this band is due to cyclobutane puckering coupled with phenyl in-plane stretching.

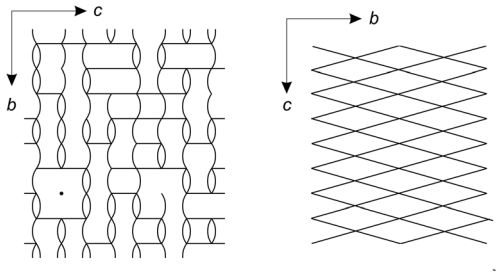

Scheme 2 Schematic of the connectivity scheme occurring within the polymeric layers in **1c** (a) and **2c** (b). Curved and straight lines denote linkers (bridging ligands are products of photocyclization) connecting the nodes (Fe(II) ions).

SC-XRD studies. Single-crystal X-ray diffraction studies revealed that irradiation of the crystal for 10 s (365 nm, 1 W) starts triggering cyclization. As the exposure time increases, the contribution of the cyclobutane product increases. After approximately 120 s, the process monitored on the single crystal is completed. Further irradiation causes the crystal quality to begin to deteriorate. It is expected that photocyclization should be more privileged along the *c* direction because of the shorter separation between coumarin fragments and less pronounced twist. This leads to the formation of polymeric chains in which neighboring Fe(II) ions are bridged by dimerized ligand molecules. Nevertheless, it was established that cyclization occurs not only in the topochemically preferred *c* direction but also in the *b* direction, in which the centers of double bonds of lactone rings are separated at nearly 4 Å. Moreover, the parallel-oriented lactone rings are twisted at about 43° (Fig. S2). In such a scenario, the coumarin molecules linking Fe(II) arranged along the *c* direction compete with coumarin fragments linking Fe(II) ions in the *b* direction (Fig. S5). Using a model that describes the disorder resulting from the presence of both the monomeric ligand molecule and its dimerized form, the partial contributions of **L1** in the *b* and *c* directions were determined. The estimated contribution of the dimers in the preferred *c* direction is 0.36 and is about three times greater than that in the alternative *b* direction (the occupancy factor for the dimer is 0.12). Hence, it excludes formation of regular polymeric layer, composed only from four-connected nodes. Based on the determined structure of **1c**, the ratio of monomer to dimer molecules is 1 to 0.47. It is worth noting that ^{1}H NMR of the bulky sample of **1c** dissolved in deuterated acetonitrile/deuterated water (20/1 v/v, see SI for details) indicates that the molar ratio of monomeric ligand molecule **L1** to the dimeric form (being the product of photoconversion) is equal to 1 : 0.42. This confirms that competition occurs in two directions, reducing the yield of the dimeric form. In such a case, the formation of various types of nodes with lower connectivity cannot be excluded and includes complex cations that are not engaged in photoconversion (Scheme 2a).

Spin-crossover properties of 1c

Photocyclization studies on a macroscopic sample of **1** enriched with ^{57}Fe (8%) were performed using Mössbauer spectroscopy. After illumination of sample **1** at 275 K for 24 h with light of λ = 365 nm (light power 10 mW, distance 80 mm), the measurements of Mössbauer spectra at 140 K (Fig. S3f) revealed the appearance of an LS component, indicating greater stabilization of the LS form.

1 → **1c** photoconversion does not lead to a change in the pattern of the spectrum (Fig. S3). Quadrupole splitting and isomer shift parameters for photoconverted sample **1c** in the HS form (ΔE_Q = 1.39 mm s^{-1}, δ = 1.05 mm s^{-1} at 240 K) and in the LS form (ΔE_Q = 0.30 mm s^{-1}, δ = 0.55 mm s^{-1} at 61 K) change insignificantly. The temperature dependence of the relative area of the HS form ($A_{HS}/(A_{HS} + A_{LS})$) indicates that spin crossover became more gradual and shifted to lower temperatures. Spin-crossover temperature $T_{1/2}$ derived from Mössbauer spectroscopy studies can be estimated to be 138 K (Fig. S4).

The results of the magnetic studies confirmed that a more gradual spin crossover occurred after photoconversion, which shifted to slightly lower temperatures ($T_{1/2}$ = 138 K) (Fig. 1).

The FTIR spectra of the macroscopic samples **1** and **1c** (nujol mull) are placed in the SI, as shown in Fig. S6.

The spin states of **1** and **1c** can be switched by irradiation with green light (λ = 532 nm, Fig. S7). The LS → HS* switching is complete. For both compounds, a similar stability of the metastable HS* phase is observed after switching. The systems begin to relax back to the LS phase above a temperature of ~30 K. In the case of compound **1c**, for which the thermally induced spin crossover shifts to slightly lower temperatures, the T_{LIESST} value is 56 K and is slightly higher compared to compound **1**, for which T_{LIESST} = 52 K. It is worth noting that, in this case, irradiation of **1** did not involve [2 + 2] cyclization.

Conclusions drawn from structural studies on photoconversion may allow for further rationalization of the spin-crossover behavior in **1c**. In light of the SCXRD studies, crystal **1c** is composed of structurally different spin-crossover centers. Moreover, the diffraction pattern does not reveal the occurrence of long-range ordering of photocyclized molecules. This implies that the nonequivalence of spin-crossover centers, in combination with the structural variability of further coordination spheres, is translated on the course of spin crossover. This results in a wider range of temperatures at which spin crossover occurs. Single-crystal X-ray diffraction studies of **1c** revealed that in the cooling mode, spin crossover starts at a temperature practically the same as that observed for **1**, whereas at lower temperatures, a significantly greater contribution of the HS form occurs. The value of $T_{1/2}$ can be estimated from single-crystal X-ray diffraction studies, which is equal to about 141 K (Fig. 1).

Spin-crossover properties of [Fe(L1)$_6$](ClO$_4$)$_2$ (2)

Studies on the temperature dependence of the magnetic susceptibility showed that cooling (1 K min^{-1}) below 100 K involves an abrupt spin-crossover ($T^1_{1/2}$ = 83 K). Further cooling below 80 K leads to a half spin-crossover, and $\chi_M T$ value remains in the range of 1.7–1.8 cm^3 K mol^{-1} (Fig. 4a). Additionally, fast cooling with a temperature speed rate of 4 K min^{-1} does not significantly change the course of spin crossover. In contrast, reducing the temperature scan rate to 0.01 K min^{-1} involves occurrence below 80 K per second, which is a very sharp and practically complete transition ($T^2_{1/2}$ = 62 K). Concomitantly, at very slow cooling, the transition observed at $T^1_{1/2}$ = 83 K remains practically unchanged. Thus, **2** exhibits a two-step spin-crossover with a pseudo-plateau in the range of 70–80 K.

In the heating mode (1 K min^{-1}), the low-temperature, second step of spin crossover is shifted to higher temperatures ($T^2_{1/2}$ = 70 K), while the spin-crossover temperature for the first step ($T^1_{1/2}$ = 83 K) practically remains the same as that observed in the cooling mode. Nevertheless, measurements performed in the settling mode during cooling and heating revealed that upon heating, the course in the second stage is practically the same as that obtained in the cooling cycle. Thus, the presence of the hysteresis loop in the second step results from the slow kinetics of the spin crossover (Fig. 4b).

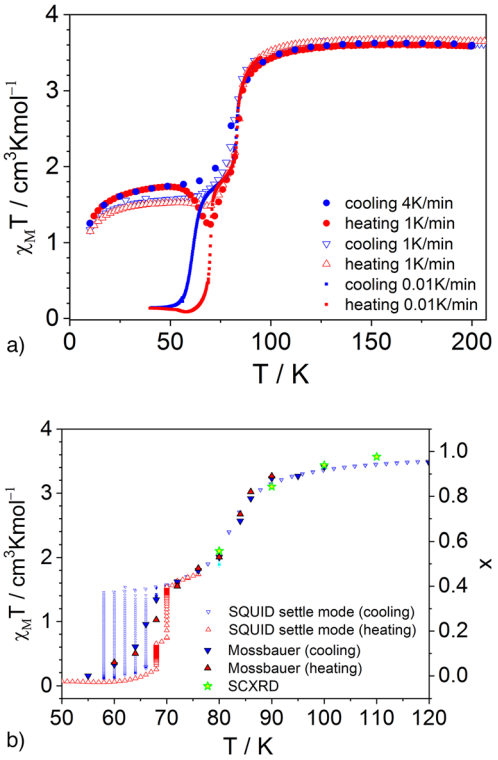

Fig. 4 $\chi_M T(T)$ dependencies for **2** recorded at various temperatures and speed rates (a). Results of magnetic studies in the time-resolved mode, together with temperature dependences of the relative areas of the HS form derived from Mössbauer spectroscopy and the contribution of the HS form derived from single-crystal X-ray diffraction studies (b). x is defined for Mössbauer spectroscopy according to $A_{HS}/(A_{HS} + A_{LS})$, while for SCXRD, it is $(d^T_{Fe-N} - d^{LS}_{Fe-N})/(d^{HS}_{Fe-N} - d^{LS}_{Fe-N})$, where d is the average Fe–N distance determined at temperature T for the HS and LS forms.

Spin-state switching in **2** can also be accomplished by light (Fig. S8). Irradiation of the LS form (obtained by the previous thermal HS → LS switching carried out at 60 K, followed by cooling to 10 K) with light of a wavelength of 532 nm results in quantitative LS → HS* switching. Heating (0.3 K min^{-1}) generates the HS* form, which triggers HS* → LS conversion at temperatures above 50 K. For a change, cooling sample **2** to 10 K with a temperature scan rate of 1 K min^{-1} leads to nearly equal contributions of the HS and LS forms. In such a case, relaxation to the HS or LS form is not observed at 10 K. This allows for switching the sample with 532 nm light to the HS* form or illuminating the sample with 808 nm to the LS form. Irradiation with red light leads to a sample containing about 20% of the HS form, and just further heating (0.3 K min^{-1}) causes (above 50 K) vanishing of the HS form as expected.

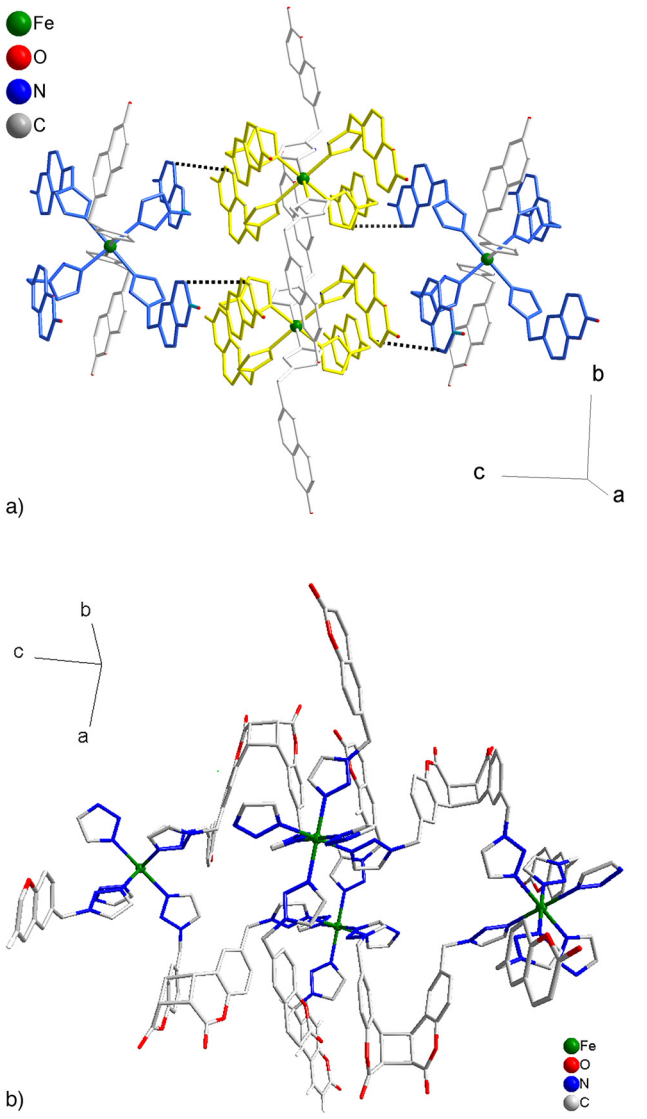

Fig. 5 Arrangement of $[FeL_6]^{2+}$ cations within the *bc* plane in **2** (a) and in the product of photocyclization **2c** (b). Blue- and yellow-colored fragments joined by black dotted lines denote molecules that meet the topochemical conditions, while the ligands marked in grey color (a) do not participate in the photoconversion.

The first coordination sphere in **2** is composed of six 1,2,3-triazole rings (Fig. 5a, Fig. S9a), similar to that in **1**. At 250 K, the Fe–N distances are equal to 2.228(1), 2.213(1) and 2.168(1) Å. The N–Fe–N angles are in the range of 87.8(1)°–92.2(1)°. There are therefore no differences in the structure of FeN_6 chromophores between **1** and **2** that unambiguously explain the differences in spin-crossover temperatures.

Variable temperature single-crystal X-ray diffraction studies showed that lowering the temperature below 100 K involves shortening the Fe–N distances (Fig. 4b). At 80 K, the Fe–N distances are equal to 2.122(2), 2.134(3) and 2.079(3) Å, so the contribution of the HS form can be estimated to be about 55% (considering an expected shortening of the Fe–N distance by ~0.2 Å). At 80 K, there are no major changes in the structure of the complex cation in relation to the HS structure. The orientation of the ligand molecules with respect to the FeN_6 chromophore remains practically unchanged. The changes in torsion angles do not exceed 3° (Table S4).

It is worth mentioning that in the HS phase (250 K), there is one crystallographically independent iron atom in the crystal lattice. This does not change at 80 K, where one crystallographically independent iron atom in the crystal lattice is still present. Moreover, at this temperature, no other structural changes were observed compared to the structure determined at 250 K. Some light on why a two-step spin-crossover occurs in **2** is shed by the results of the Mössbauer spectroscopy studies. Above the spin-crossover temperature region, the spectrum consists of a quadrupole doublet (ΔE_Q = 2.05 mm s^{-1}, δ = 1.14 mm s^{-1} at 200 K) corresponding to the HS form (Fig. S10a). Cooling below 140 K is associated with the appearance of a signal consisting of two LS components. At the saddle point (76 K), the contribution of the HS form (derived from the ratio of the experimental areas according to $A_{HS}/(A_{HS} + A_{LS1} + A_{LS2})$) equals 0.48 (Fig. 6a). At 50 K, only low spin components (Fig. S10b) of areas ratio $A_{LS1}:A_{LS2}$ – 1 : 1 (δ_{LS1} = 0.53 mm s^{-1}, $\Delta E_{Q(LS2)}$ = 0.30 mm s^{-1}, δ_{LS2} = 0.55 mm s^{-1}) are present. Thus, the evolution of Mössbauer spectra indicates the occurrence of structural changes within the temperature range of the spin crossover, which can be responsible for a two-step character. In the heating mode, spin crossover shifts to slightly higher temperatures, which, in accordance with magnetic studies, confirms that the second step is associated with the occurrence of a very narrow hysteresis loop of width *ca.* 2 K (Fig. 4b).

Photoconversion studies 2 → 2c

In compound **1**, four ligand molecules interact with two neighboring molecules arranged in one direction along the *b* axis. However, a one-dimensional polymeric structure was not formed because there exists competition with coumarin fragments originating from neighboring supramolecular columns (along the *c* direction). In the case of compound **2**, the arrangement of the photoreactive fragments is completely different. Here, four ligand molecules (coumarin fragments) are directed

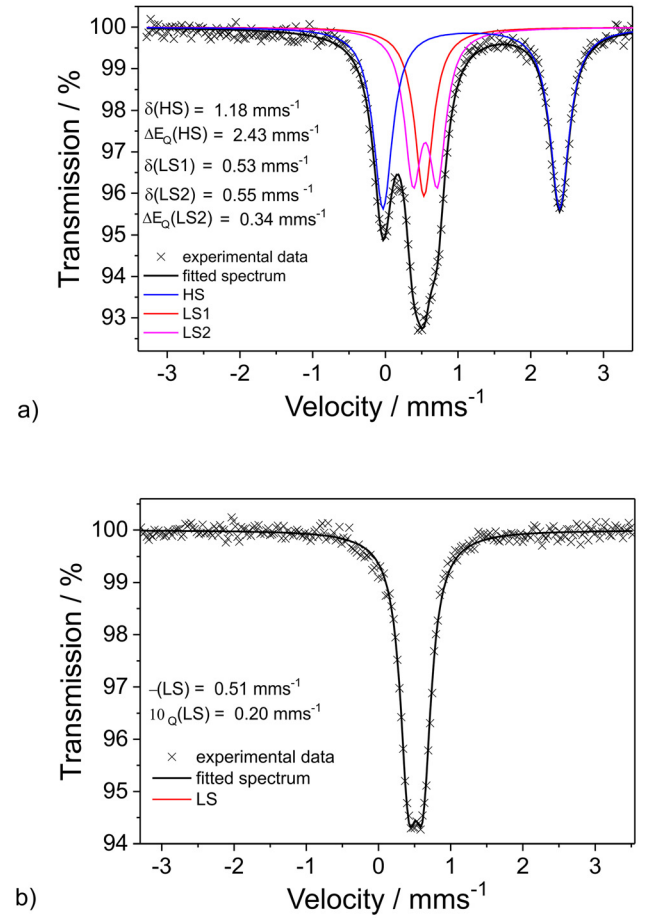

Fig. 6 Mössbauer spectra of **2** (a) and **2c** (b) recorded at 76 and 80 K, respectively.

into four complex cations coplanarly arranged in the *bc* plane (Fig. 5a). Within this supramolecular layer, each cation interacts with four neighboring ones through stacking interactions of the coumarin fragments. The distances between the centers of the double bonds of the lactone rings are the same, adopting a value of 3.64 Å. In contrast to **1**, the two remaining coumarin fragments in **2** do not meet the topochemical requirements.

FTIR microscopy. Preliminary studies of the ability of compound **2** to undergo [2 + 2] photocyclization were performed using FTIR microscopy. Additionally, in this case, irradiation (λ = 365 nm) of a very thin crystalline plate involves changes in the spectra. It occurs in the range of 1150–1350 cm^{-1} (Fig. 3b) and is more pronounced in comparison with **1**. In comparison to photoconversion **1** → **1c**, irradiation of **2** leads to the appearance of a new peak at 1324 cm^{-1}. Additionally, the shape of the ν(C=O) band changes, with an additional peak emerging at 1739 cm^{-1}. Notably, the characteristic ν(CN) vibration at 2250 cm^{-1} is absent (Fig. 3b, Fig. S11).

SC-XRD studies. The complete [2 + 2] cycloaddition caused by irradiation (λ = 365 nm, 1 W) of a single crystal (0.08 × 0.20 × 0.38 mm^3) was accomplished within 80 s. Thus, only four coumarin fragments, fulfilling the topochemical requirements, were photoconverted (Fig. 5b, Fig. S9b). Contrary to **1**, the process occurs in **2** quantitatively and results in the formation of polymeric layers of the rhombic grid (Scheme 2b).

Cycloaddition is accompanied by the formation of a cyclobutane ring. In previous studies, we determined the crystal structure of the uncoordinated form of a dimeric, tetrazole-based ligand.[24] The torsion angle defined by four carbon atoms of the cyclobutane in such a dimeric ligand molecule was equal to 17.9(1)°, while in the high-spin form of the coordination compound, it (C2–C3–C14–C13) was 13.3(1)°, indicating the appearance of some strain. The values of the puckering angles were equal to 25.3° and 19.3° (80 K). The situation in **2c** changes dramatically. The cyclobutane ring is significantly more flattened. The torsion angle (C14–C15–C27–C26) equals only 8.4(1)°, while the puckering angle adopts a value of 11.8° (300 K) (transition to the LS form involves an increase in the angle to 12.4° at 80 K). It is worth noting that for a stress-free cyclobutane derivative, one expects a value of about 25–30°. This means that the dimeric molecule in complex **2c** is extremely strained. For comparison in **2**, the torsion angles defined by the carbon atoms of the cyclobutane rings are equal to 21.2° and 35.2° (HS, 250 K). The puckering angles adopt values of 27.5° and 46.4°, respectively. Without a doubt, the structure of the cyclobutane fragment is different from that of other coumarin derivatives.

In contrast to other coumarin-based photo-products, the methylene group in **2c** is directed towards the carbon atom of the 1,2,3-triazole ring from the adjacent arm of the same dimeric ligand molecule. The $C_{tr}\cdots C_{methylene}$ distance is 3.36(1) Å; thus, it is shorter than the sum of the van der Waals radii for carbon atoms. Moreover, distances between hydrogen atoms are equal to 2.1 Å (HS form) and 2.0 Å (LS form), that is, they are shorter than the sum of van der Waals radii for hydrogen atoms, too. Therefore, the strain in **2c** may also result from repulsive interactions. For comparison, from the previously studied tetrazole derivative to compound **2c**, the tetrazole nitrogen atom N1 is replaced by the corresponding carbon atom C_{tr} in the 1,2,3-triazole ring; hence, the nitrogen atom in the tetrazole derivative could participate in an attractive interaction (Fig. S14). Importantly, the corresponding $C_{tr}\cdots C_{methylene}$ distance in **2** exceeds 3.6 Å.

Attempts to reverse the photocycloaddition by exposing **2c** to UV light (250–260 nm) were unsuccessful. Heating was also attempted. It was determined that the dissociation process begins at 225–230 °C. The crystal structure determination revealed ligand disorder, with both the dimeric form and the reconstructed initial monomer present at the same Fe(II) coordination site. Based on the occupancy factors, it was established that approximately 10% of the dimeric ligand molecules had dissociated. Due to the presence of perchlorates, work on bulky samples and at higher temperatures was not conducted.

Spin-crossover properties of 2c

A bulky sample of the product of photoconversion **2c** was prepared by irradiation (365 nm, light power 10 mW, distance

80 mm) of a very thin layer of **2** under Mössbauer spectroscopy monitoring. It was established that photoconversion **2** → **2c** starts at a very low temperature, that is, at 140 K (Fig. S13a). Importantly, at this temperature, **2** remains in the HS form. Thus, irradiation triggers HS → LS switching, and after 24 h of illumination, 40% of HS form remains. Further irradiation at this temperature increased the LS fraction. Therefore, the temperature was elevated to 250 K, and irradiation continued for 48 h. After that time, the sample was cooled to 140 K, and the recorded spectrum indicated the presence of only the LS form (Fig. S13b). After complete spin-state switching triggered by ligand photoconversion, the sample was heated to 300 K, and variable-temperature Mössbauer spectroscopy was carried out in the cooling mode. At 250 K, the spectrum shows one doublet with $\Delta E_{Q(HS)}$ = 2.09 mm s^{-1} and δ_{HS} = 1.10 mm s^{-1}. Below this temperature, a HS → LS transition starts centered at $T_{1/2}$ = 197 K and is completed at 140 K. In the spin-crossover temperature region, only one component is present, which is characteristic of the LS form ($\Delta E_{Q(LS)}$ = 0.20 mm s^{-1}, δ_{LS} = 0.51 mm s^{-1}). Further cooling does not involve changes in the pattern of the spectrum.

Magnetic measurements were performed on the sample generated as described above, and the recorded $\chi_M T(T)$ dependence was consistent with that obtained from Mössbauer studies. No hysteresis was found (Fig. 7). Continuous irradiation of sample **2c** at 10 K with 532 nm light leads to LS → HS* switching (Fig. S14). However, immediately after turning the light off, HS* → LS relaxation starts. Considering the significant elevation of $T_{1/2}$, the low efficiency of photoswitching remains in agreement with the inverse energy gap law.[29,30]

To sum up, surprisingly, the spin crossover was significantly shifted towards higher temperatures from *ca.* 83 to 197 K, *i.e.*, at about 114 K. To the best of our knowledge, such behavior was not previously observed for other spin-crossover systems based on photoresponsive ligands. The first successful application of the [2 + 2] photocycloaddition was presented by M.-L. Tong by irradiating the Hoffman network-type systems $[Fe(4\text{-spy})_2\{Ag(CN)_2\}_2]$ and $[Fe(2,4\text{-bpe})_2\{Ag(CN)_2\}_2]$ (4-spy = 4-styrylpyridine, 2,4-bpe = *trans*-1-(2-pyridyl)-2-(4-pyridyl)ethylene) with UV light (high-pressure mercury lamp).[23] In the first case, an abrupt and complete spin-crossover ($T_c^{\downarrow}$ = 212 K and $T_c^{\uparrow}$ = 215 K) changes character to a two-step one and shifts to lower temperatures ($T_{c1}^{\downarrow}$ = 190 K, $T_{c1}^{\uparrow}$ = 194 K, $T_{c2}^{\downarrow}$ = 166 K and $T_{c2}^{\uparrow}$ = 169 K). For the second compound, the two-step spin-crossover ($T_{c1}^{\downarrow}$ = 164 K, $T_{c1}^{\uparrow}$ = 167 K, $T_{c2}^{\downarrow}$ = 141 K and $T_{c2}^{\uparrow}$ = 146 K) becomes incomplete and occurs over a broad temperature range from 50 to 300 K. Further research by the same group using photoreactive ligands of the styrylpyridine type resulted in another Hoffman network-type system $[Fe(3\text{-spy})_2\{Pd(CN)_4\}]$ (1,3-spy = 3-styrylpyridine) exhibiting a two-step spin transition ($T_{c1}^{\downarrow}$ = 123 K and $T_{c1}^{\uparrow}$ = 132 K and $T_{c2}^{\downarrow}$ = 94 K and $T_{c2}^{\uparrow}$ = 119 K).[22] In this case, quantitative photoconversion leads to a high-spin system. It is worth noting that the photocycloaddition process could be reversed by 68% by heating at 250 K for 12 h. Further studies using 3-spy led to the synthesis of $[Fe(3\text{-spy})_2\{Ag(CN)_2\}_2]$ undergoing a two-step spin transition below 150 K.[31] Photocycloaddition [2 + 2] results in a gradual and incomplete spin-crossover occurring in the range of 70–200 K. Irradiating the photoconversion product with 254 nm UV light allows for the partial reversal of the cycloaddition. Our recent studies demonstrated that the use of 7-(tetrazol-2-ylmethyl)coumarin leads to a mononuclear system, $[Fe(\mathbf{L})_6](BF_4)_2{\cdot}4CH_3CN$, exhibiting a cooperative and complete spin-crossover (T_c = 130 K), while the high-spin product of [2 + 2] photocycloaddition did not show a thermally induced spin-crossover.[24] It is worth noting that coordination compounds containing ligands undergoing intramolecular photoisomerization attract immense interest. A review of such systems was conducted by B. Brachňaková and I. Šalitroš.[32]

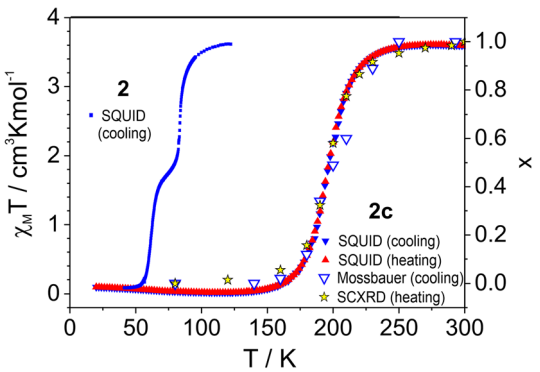

Fig. 7 Temperature dependences of $\chi_M T$ (SQUID, 1 K min^{-1}), relative areas of the HS form derived from Mössbauer spectroscopy and relative shortening of average Fe–N distance derived from single-crystal X-ray diffraction studies for **2c**. The meaning of *x* is given in the caption to Fig. 4. For comparison, the $\chi_M T(T)$ curve (cooling mode, 0.01 K min^{-1}) for compound **2** (blue squares) is added.

The average molar ratio of ligand molecules that underwent photocycloaddition (dimers) to molecules that did not undergo conversion was determined from the ^{1}H NMR spectrum (sample **2c**) dissolved in deuterated acetonitrile/deuterated water (20/1 v/v, see SI for details) based on the integration of signals from the methylene group protons, which were completely separated in the spectrum. The determined molar ratio is 1.92 : 1.

Structural effect of photocycloaddition on the spin-crossover properties of complex 2c. In the HS form of **2c**, the distance between bridged Fe(II) ions equals 12.00 Å at 300 K, while the separation between the corresponding metal ions before conversion is equal to 11.92 Å. The distance between Fe(II) ions from neighboring layers expands from 18.12 Å in **2** (250 K) to 18.01 Å (300 K) in **2c**. The summary effect of intra- and interlayer expansion results in the expansion of the cell volume from 3477 Å^3 (**2**, 250 K) to 3513 Å^3 (**2c**, 300 K). Photoconversion practically does not affect the anion network.

In the HS form of **2c** at 300 K, the Fe–N bond lengths are equal to 2.225(1), 2.198(1), and 2.173(1) Å. The average Fe–N distance equals 2.199(1) Å and is insignificantly shorter than the values observed at 250 K for **2** (2.203(1) Å) and **1** (2.200(2)

Å). It should be noted that after photoconversion, Σ adopts a value of 28.9° (300 K), which is greater than the values observed for 2 (16.3° at 250 K) and **1** (14.1° at 250 K). Cooling of crystal **2c** to 250 K involves a slight shortening of the Fe–N distances to 2.212(2), 2.183(2), and 2.168(2) Å, which is in line with the start of spin crossover. At 80 K, the Fe–N bond lengths are equal to 1.973(1), 1.988(1), and 2.001(1) Å; thus, they are characteristic of the LS form. A value of Σ = 29.4° for the LS form of **2c** is close to the one found for the HS form. The temperature dependence of the Fe–N distances (Fig. 7) for **2c** agrees with the results of the magnetic and Mössbauer studies.

Spin crossover in **2c** involves a slight reorientation of triazole rings (tr). The N_{tr}–N_{tr}–Fe–N_{tr} torsion angles as well as the angles between the planes of the triazole rings and the equatorial plane of the coordination octahedron (defined by nitrogen donor atoms from ligands undergoing photoconversion) change by 1°–4° upon spin crossover in **2c**. The changes in the mutual orientation of the triazole and coumarin fragments are of similar magnitude. In **2**, these changes are smaller than 3°. The HS → LS transition in **2c** involves a reduction of the distance between bridged Fe(II) ions from 12.00 Å (300 K) to 11.73 Å (80 K, complete spin-crossover). For comparison, the corresponding separation in **2** decreases from 11.92 Å (250 K) to 11.72 Å at 80 K; *ca.* 50% of the Fe(II) ions adopt the LS state. Spin crossover also involves a decrease in the separation between the polymeric layers in **2c** from 18.01 Å to 17.71 Å. The analogous distance in **2** is reduced from 18.12 Å to 18.07 Å.

In conclusion, the structural changes associated with thermally induced spin crossover in complexes **1** and **2** as well as their photoconversion products are typical.

Our previous studies on the coordination compound $[FeL_6](FB_4)_2{\cdot}4CH_3CN$ and its photoconversion product demonstrate that the stress resulting from photoconversion is a reason for the very strong stabilization of the HS form. In fact, the photoconversion in **2c** entails much larger alterations. The **2** → **2c** conversion involves a reorientation of one of the three crystallographically independent 1,2,3-triazole rings with respect to the Fe–N6 bond; the torsion angle N8–N9–Fe–N6 increases from 32.8(2)° to 37.3(2)°. Additionally, it is associated with a change in the inclination of the triazole ring in relation to the equatorial plane of the coordination octahedron. Moving away from the Fe(triazole)$_6$ core, the adaptive abilities of the ligand molecules become more pronounced. Thus, the torsion angles covering the methylene group of the ligand molecules undergoing photocycloaddition change in a wide range of values (from 4 to 27°, Table S3). The structural transformation is also reflected in the ligand molecule not taking part in the cyclization process, which indicates the appearance of perturbation spreading on the whole crystal lattice; here, the angle N1–C10–C6–C7 changes by about 8.6°.

To sum up, it is clearly visible that the structural changes associated with the **2** → **2c** photoconversion are much greater than those resulting from the thermally induced spin-crossover. Concomitantly, a comparison of the crystal structures of **2** and **2c** indicates that the changes triggered by spin crossover in **2c** are slightly greater than those that occurred in **2**, and these changes are typical of thermally induced spin-crossover. Nevertheless, a comparison of the magnitudes and directions of these changes does not provide any basis for explaining why photoconversion leads to such strong stabilization of the LS form. Thus, it should be considered that lattice-based effects perpetuate stress and prevent stored energy from dissipating. In such a situation, the strain accumulated in the coordination compound **2c** ligand structure crucially affects the energies of the HS and LS forms, which are responsible for a drastic change in spin-crossover properties. To evaluate this effect, density functional theory (DFT) calculations were performed.

DFT calculations

We applied DFT modelling to account for the 100 K shift in the transition temperature of **2c** upon photoconversion. We performed the calculations with Gaussian 16 [33] using the TPSS exchange–correlation functional[34] and the TZVP basis set[35,36] with Grimme's D3 dispersion correction.[37] In what follows, we focus on the change in strain in the photodimerized ligand from the LS to the HS state. First, we calculated the mean electronic energies of the photodimerized ligands for the HS and LS spin isomers, taking the geometries of the two inequivalent ligands. Much lower energy was found for the ligands in the LS structures; the difference between the LS and HS states was 234 kJ mol^{-1}. To compare this value with the known difference in the strain of the ligands coordinated to the LS and HS spin isomers of the SCO Fe(II) complexes, we may refer to ref. 38. It was shown that for 17 Fe(II) spin-crossover complexes with hexa-coordinating nitrogen-donor ligands, LS–HS conversion is associated with a release of ligand stress of 95 ± 16 kJ mol^{-1}. This value implies that the LS to HS spin transition results in a significant decrease in the ligand strain in the mononuclear complexes. For the systems under study in this paper, the opposite effect is thus found. It is noteworthy that our modelling of the 1D photodimerized analogous system containing the tetrazole coordinating ligands (ref. 24) does not reveal any change in the strain of the ligands. In a further step, we calculated the strain difference of the ligands and subsequently the smaller fragments thereof (Fig. 8). The decomposition of the strain differences reveals that the largest part of the stress (energetic effect of strain) difference (102 kJ mol^{-1}) in the dimerised ligand comes from the interaction involving the triazole rings. The rest (132 kJ mol^{-1}) is the sum due to differently interacting phenyl rings (96 kJ mol^{-1}) and the difference in the conformation of cyclobutane (36 kJ mol^{-1}). The stress difference of 102 kJ mol^{-1} between the model of the ligand and its core without tetrazole ligands contains 62 kJ mol^{-1} due to the different interactions of the methyltriazole rings. Consequently, the remaining 40 kJ mol^{-1} must be due to the interactions between the triazole moieties and the phenyl rings. All interactions shown in Fig. 8 favour the geometry observed in the LS state of **2c**. This is somewhat surprising; only 15% of the additional ligand stress upon transition from the LS to the HS state is due to strain induced in the cyclobu-

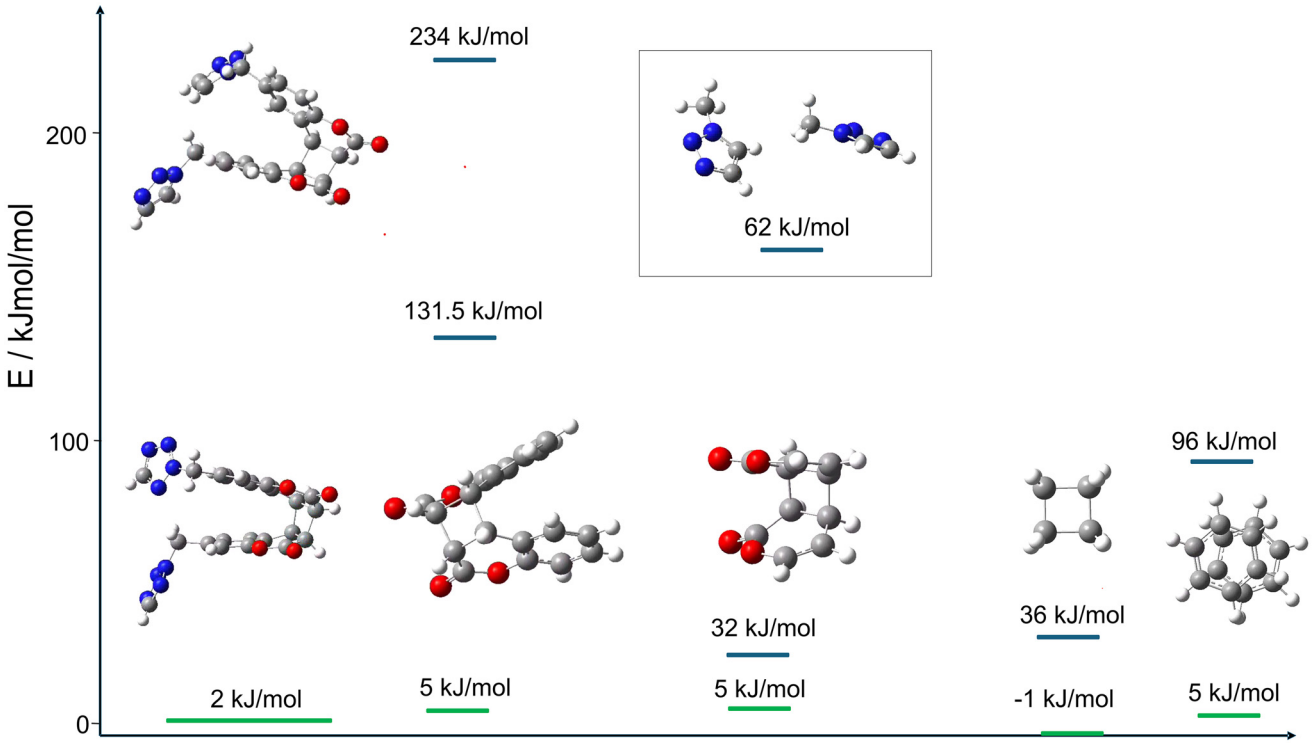

Fig. 8 Electronic energy differences ΔE of photodimerized ligands and their fragments corresponding to the whole molecules in their HS and LS states. Energy differences were taken between the HS and LS configurations ($E_{HS}-E_{LS}$). Thus, positive values reflect a higher strain for the related HS structures. Energies were calculated using single point calculations for isolated fragments with geometries taken from the X-ray data. The obtained ΔE values for the ligand of **2c** and its decomposed fragments are shown as blue bars and compared to related tetrazole analogues (ref. 24, green bars). Notably, the electronic energy of the optimized cyclobutane obtained using the same DFT tools is 145 kJ mol^{-1} higher than that obtained for the cyclobutane fragment corresponding to that in the LS structure of **2c**, indicating stress due to the compression of the cyclobutane skeleton in the dimerized ligand. Although the disorder of the coumarin cyclobutane fragment in the structure of **1c** makes it difficult to obtain reliable coordinates for computation, it was possible to calculate the stress difference related to the vicinity of the triazole ring (see the structure shown in the box). The obtained value of 38 kJ mol^{-1} is significantly lower than that for **2c**. We were also able to obtain the geometry of the cyclobutane for LS-**1c**. Although the reliability of this model is limited by two C–C bonds elongated (one being over 1.7 Å long) and the other shortened (one being below 1.4 Å), the obtained energy points to a lower strain in the dimerised ligand in **1c** than in **2c**. Moreover, the energy of this disordered cyclobutane ring is 105 kJ mol^{-1} higher than that obtained for the optimized geometry. The robustness of the calculations of the stress difference was checked using calculations with four different correlation-exchange functionals, each with four different basis sets. The results are shown in the SI and reveal fairly similar findings, revealing the weaker dependence of the calculated strain difference on the functional (the largest difference of *ca.* less than 10%) and somewhat higher on the basis set (the largest difference of less than *ca.* 20%).

tene ring. Seemingly, this ring suffers from such a large strain that additional deformation is only limitedly possible. This effect counterbalances the entropic and ligand-field effects, which are the driving forces of the LS to HS transition, resulting in a 100 K shift at the critical temperature.

Conclusions

In summary, we reported the successful application of the novel ligand 6-(1,2,3-triazol-1-ylmethyl)coumarin (**L1**) to prepare the photoreactive mononuclear coordination compounds $[Fe(\mathbf{L1})_6](ClO_4)_2{\cdot}n CH_3CN$ (n = 0, 2). An unprecedented feature of the solvated form is the presence of three photoreactive fragments, forming two types of coumarin–coumarin pairs that concomitantly meet topochemical conditions. The photocycloaddition of each pair must occur in a different direction. However, irradiation at 365 nm triggers competition between the photoreactive fragments, resulting in the formation of a frustrated structure of the polymeric layer. In effect, the more gradual spin crossover is shifted to slightly lower temperatures. This contrasts with the unsolved system, which contains two pairs of coumarin fragments that do not compete with each other. Consequently, photoconversion results in a 2D network with a regular (2,2) topology. Here, we observe that the spin crossover shifts by 114 K towards higher temperatures, which, to the best of our knowledge, has not been observed for photoconvertible systems. A characteristic feature of the photoconverted system is the presence of a strained form of the resulting bridging ligand molecule in which the cyclobutane ring is extremely strongly flattened; the puckering angle is equal to 11.8°. DFT modelling of the strain in the photodimerized ligand points towards much higher stress in the HS state. Considering that similar coordination with two photodimer-

ized and two non-dimerized ligands forms the 1D chains with the tetrazole analogues, it seems that it is primarily the 2D topology of the lattice of **2c** that induces these effects.

Author contributions

M. K. performed compounds synthesis, photoconversion experiments, FTIR microscopy measurements, data processing, analysis and interpretation of the data, presentation of the results, contributed to the finalization of the manuscript. M. W. collected the magnetic susceptibility data. M. S. collected the single-crystal X-ray diffraction data for compound **2** at 80 K. V. M. performed the crystal structure determination. A. T. assisted with the synthesis of the compounds. V. S. and J. A. W. performed the DFT modelling and discussed the DFT results. R.B. supervised the project, provided financial support, prepared the manuscript, and collected the Mössbauer spectroscopy data.

Conflicts of interest

There are no conflicts to declare.

Data availability

Supplementary information (SI): the experimental section, supporting data, computational analysis and movies. See DOI: **https://doi.org/10.1039/d5qi02305j**.

CCDC 2490226–2490234 contain the supplementary crystallographic data for this paper.[39a–i]

Acknowledgements

R. B. is grateful to the University of Wrocław for financial support (BPIDUB.14.2024). V. S. and J. A. W. acknowledge the support by the Deutsche Forschungsgemeinschaft (DFG) through CRC/TRR173, "Spin + X", project A4. V. S. also acknowledges support by the German Ministry of Research (BMBF) under 05K22UK1 and the research initiative NanoKat. J. A. W. and V. S. are grateful to the Allianz für Hochleistungsrechnen Rheinland–Pfalz (AHRP) for providing CPU time under the project RPTU-SPINPLUSXA4.

References

1 C. Bao, P. Tang, D. Sun and S. Zhou, Light-induced emergent phenomena in 2D materials and topological materials, *Nat. Rev. Phys.*, 2022, **4**, 33.
2 J. J. Vittal, Supramolecular structural transformations involving coordination polymers in the solid state, *Coord. Chem. Rev.*, 2007, **251**, 1781.
3 P. Gütlich, A. Hauser and H. Spiering, Thermal and Optical Switching of Iron(II) Complexes, *Angew. Chem., Int. Ed. Engl.*, 1994, **33**, 2024.
4 A. Halcrow, *Spin-Crossover Materials: Properties and Applications*, Wiley-VCH, Weinheim, 2013.
5 P. Guionneau, M. Marchivie, G. Bravic, J.-F. Letard and D. Chasseau, Structural Aspects of Spin Crossover. Example of the (FeIILn (NCS) 2) Complexes, *Top. Curr. Chem.*, 2004, **234**, 97.
6 M. Seredyuk, A. B. Gaspar, V. Ksenofontov, Y. Galyametdinov, J. Kusz and P. Gütlich, Does the solid–liquid crystal phase transition provoke the spin-state change in spin-crossover metallomesogens?, *J. Am. Chem. Soc.*, 2008, **130**, 1431.
7 M. Seredyuk, M. C. Muñoz, M. Castro, T. Romero-Morcillo, A. B. Gaspar and J. A. Real, Unprecedented multi-stable spin crossover molecular material with two thermal memory channels, *Chem. – Eur. J.*, 2013, **19**, 6591.
8 M. Książek, M. Weselski, A. Dreczko, V. Maliuzhenko, M. Kaźmierczak, A. Tołoczko, J. Kusz and R. Bronisz, Two ways of spin crossover in an iron(II) coordination polymer associated with conformational changes of a bridging ligand, *Dalton Trans.*, 2020, **49**, 9811.
9 R. Akiyoshi, R. Ohtani, L. F. Lindoy and S. Hayami, Spin crossover phenomena in long chain alkylated complexes, *Dalton Trans.*, 2021, **50**, 5065.
10 M. Weselski, M. Książek, P. Mess, J. Kusz and R. Bronisz, "Normal" and "reverse" spin crossover induced by two different structural events in iron(II) coordination polymer, *Chem. Commun.*, 2019, **55**, 7033.
11 M.-L. Boillot, J. Zarembowitch and A. Sour, Ligand-driven light-induced spin change (LD-LISC): a promising photomagnetic effect, *Top. Curr. Chem.*, 2004, **234**, 261.
12 M.-L. Boillot, C. Roux, J.-P. Audière, A. Dausse and J. Zarembowitch, Ligand-Driven Light-Induced Spin Change in Transition-Metal Complexes: Selection of an Appropriate System and First Evidence of the Effect, in FeII (4-styrylpyridine)$_4$(NCBPh$_3$)$_2$, *Inorg. Chem.*, 1996, **35**, 3975.
13 M.-L. Boillot, S. Pillet, A. Tissot, E. Rivière, N. Claiser and C. Lecomte, Ligand-driven light-induced spin change activity and bidirectional photomagnetism of styrylpyridine iron(II) complexes in polymeric media, *Inorg. Chem.*, 2009, **48**, 4729.
14 L. Poggini, G. Londi, M. Milek, A. Naim, V. Lanzilotto, B. Cortigiani, F. Bondino, E. Magnano, E. Otero, P. Sainctavit, M.-A. Arrio, A. Juhin, M. Marchivie, M. M. Khusniyarov, F. Totti, P. Rosa and M. Mannini, Room temperature control of spin states in a thin film of a photochromic iron(II) complex, *Mater. Horiz.*, 2018, **5**, 506.
15 Y. Hasegawa, K. Takahashi, S. Kume and H. Nishihara, Complete solid state photoisomerization of bis (dipyrazolylstyrylpyridine) iron(II) to change magnetic properties, *Chem. Commun.*, 2011, **47**, 6846.
16 M. Nihei, Y. Suzuki, N. Kimura, Y. Kera and H. Oshio, Bidirectional Photomagnetic Conversions in a Spin–

Crossover Complex with a Diarylethene Moiety, *Chem. – Eur. J.*, 2013, **19**, 6946.
17 M. Milek, F. W. Heinemann and M. M. Khusniyarov, Spin crossover meets diarylethenes: efficient photoswitching of magnetic properties in solution at room temperature, *Inorg. Chem.*, 2013, **52**, 11585.
18 B. Resner, M. Milek, A. Witt, B. Gobaut, P. Torelli, R. H. Fink and M. M. Khusniyarov, Reversible Photoswitching of a Spin–Crossover Molecular Complex in the Solid State at Room Temperature, *Angew. Chem., Int. Ed.*, 2015, **54**, 12976.
19 M. Estrader, J. S. Uber, L. A. Barrios, J. Garcia, P. Lloyd-Williams, O. Roubeau, S. J. Teat and G. Aromi, A Magneto–optical Molecular Device: Interplay of Spin Crossover, Luminescence, Photomagnetism, and Photochromism, *Angew. Chem., Int. Ed.*, 2017, **56**, 15622.
20 K.-P. Xie, Z.-Y. Ruan, B.-H. Lyu, X.-X. Chen, X.-W. Zhang, G.-Z. Huang, Y.-C. Chen, Z.-P. Ni and M.-L. Tong, Guest–driven light–induced spin change in an azobenzene loaded metal–organic framework, *Angew. Chem., Int. Ed.*, 2021, **60**, 27144.
21 V. Kumar, A. Rotaru and Y. Garcia, Room temperature light induced spin state switching in a Fe II coordination polymer featuring a photo responsive anion, *J. Mater. Chem. C*, 2022, **10**, 14128.
22 L.-F. Wang, B.-H. Lv, F.-T. Wu, G.-Z. Huang, Z.-Y. Ruan, Y.-C. Chen, M. Liu, Z.-P. Ni and M.-L. Tong, Reversible on-off switching of spin-crossover behavior via photochemical [2 + 2] cycloaddition reaction, *Sci. China: Chem.*, 2022, **65**, 120.
23 L.-F. Wang, W.-M. Zhuang, G.-Z. Huang, Y.-C. Chen, J.-Z. Qiu, Z.-P. Ni and M.-L. Tong, Spin-crossover modulation via single-crystal to single-crystal photochemical [2 + 2] reaction in Hofmann-type frameworks, *Chem. Sci.*, 2019, **10**, 7496.
24 M. Kaźmierczak, M. Weselski, M. Siczek, J. A. Wolny, V. Schünemann and R. Bronisz, [2 + 2] Photocyclization converts thermally induced spin crossover effect into "hidden hysteresis" one, *Chem. Sci.*, 2025, **16**, 7884.
25 G. M. J. Schmidt, Photodimerization in the solid state, *Pure Appl. Chem.*, 1971, **27**, 647.
26 Z. Savion and D. L. Wernick, Monomer environments during the solid-state photodimerization of trans-p-bromocinnamic acid, *J. Org. Chem.*, 1993, **58**, 2424.
27 V. Enkelmann, G. Wegner, K. Novak and K. B. Wagener, Single-crystal-to-single-crystal photodimerization of cinnamic acid, *J. Am. Chem. Soc.*, 1993, **115**, 10390.
28 K. Gnanaguru, N. Ramasubbu, K. Venkatesan and V. Ramamurthy, A study on the photochemical dimerization of coumarins in the solid state, *J. Org. Chem.*, 1985, **50**, 2337.
29 A. Hauser, Reversibility of light-induced excited spin state trapping in the $Fe(ptz)_6(BF_4)_2$, and the $Zn_{1-x}Fe_x(ptz)_6(BF_4)_2$ spin-crossover systems, *Chem. Phys. Lett.*, 1986, **124**, 543.
30 A. Hauser, Intersystem crossing in the $[Fe(ptz)_6](BF_4)_2$ spin crossover system (ptz=1-propyltetrazole), *J. Chem. Phys.*, 1991, **94**, 2741.
31 L.-F. I. Wang, L. Wu, G.-Z. Huang, S.-G. Wu and M.-L. Tong, Photochemical [2 + 2] reaction-tuned spin-crossover cooperativity in an Fe(II)–Ag(I) bimetallic Hofmann-type framework, *Inorg. Chem. Front.*, 2025, **12**, 5710.
32 B. Brachňaková and I. Šalitroš, Ligand-driven light-induced spin transition in spin crossover compounds, *Chem. Pap.*, 2018, **72**, 773.
33 M. J. Frisch, G. W. Trucks, H. B. Schlegel, G. E. Scuseria, M. A. Robb, J. R. Cheeseman, G. Scalmani, V. Barone, G. A. Petersson, H. Nakatsuji, X. Li, M. Caricato, A. V. Marenich, J. Bloino, B. G. Janesko, R. Gomperts, B. Mennucci, H. P. Hratchian, J. V. Ortiz, A. F. Izmaylov, J. L. Sonnenberg, D. Williams-Young, F. Ding, F. Lipparini, F. Egidi, J. Goings, B. Peng, A. Petrone, T. Henderson, D. Ranasinghe, V. G. Zakrzewski, J. Gao, N. Rega, G. Zheng, W. Liang, M. Hada, M. Ehara, K. Toyota, R. Fukuda, J. Hasegawa, M. Ishida, T. Nakajima, Y. Honda, O. Kitao, H. Nakai, T. Vreven, K. Throssell, J. A. Montgomery Jr., J. E. Peralta, F. Ogliaro, M. J. Bearpark, J. J. Heyd, E. N. Brothers, K. N. Kudin, V. N. Staroverov, T. A. Keith, R. Kobayashi, J. Normand, K. Raghavachari, A. P. Rendell, J. C. Burant, S. S. Iyengar, J. Tomasi, M. Cossi, J. M. Millam, M. Klene, C. Adamo, R. Cammi, J. W. Ochterski, R. L. Martin, K. Morokuma, O. Farkas, B. Foresman, and D. J. Fox, *Gaussian 16, Revision A.03*, Gaussian, Inc., Wallingford CT, 2016.
34 J. M. Tao, J. P. Perdew, V. N. Staroverov and G. E. Scuseria, Climbing the density functional ladder: Nonempirical meta–generalized gradient approximation designed for molecules and solids, *Phys. Rev. Lett.*, 2003, **91**, 146401.
35 A. Schaefer, H. Horn and R. Ahlrichs, Fully optimized contracted Gaussian basis sets for atoms Li to Kr, *J. Chem. Phys.*, 1992, **97**, 2571.
36 A. Schaefer, C. Huber and R. Ahlrichs, Fully optimized contracted Gaussian basis sets of triple zeta valence quality for atoms Li to Kr, *J. Chem. Phys.*, 1994, **100**, 5829.
37 S. Grimme, J. Antony, S. Ehrlich and H. Krieg, A consistent and accurate ab initio parametrization of density functional dispersion correction (DFT-D) for the 94 elements H-Pu, *J. Chem. Phys.*, 2010, **132**, 154104.
38 J. A. Wolny, H. Paulsen, J. J. McGarvey, R. Diller, V. Schünemann and H. Toftlund, Fe(II) complex with the octadentate btpa ligand: a DFT study on a spin-crossover system that reveals two distinct high-spin states, *Phys. Chem. Chem. Phys.*, 2009, **11**, 7562.
39 (*a*) CCDC 2490226: Experimental Crystal Structure Determination, 2026, DOI: **10.5517/ccdc.csd.cc2pl8wg**; (*b*) CCDC 2490227: Experimental Crystal Structure Determination, 2026, DOI: **10.5517/ccdc.csd.cc2pl8xh**; (*c*) CCDC 2490228: Experimental Crystal Structure Determination, 2026, DOI: **10.5517/ccdc.csd.cc2pl8yj**; (*d*) CCDC 2490229: Experimental Crystal Structure

Determination, 2026, DOI: 10.5517/ccdc.csd.cc2pl8zk; (*e*) CCDC 2490230: Experimental Crystal Structure Determination, 2026, DOI: 10.5517/ccdc.csd.cc2pl90m; (*f*) CCDC 2490231: Experimental Crystal Structure Determination, 2026, DOI: 10.5517/ccdc.csd.cc2pl91n; (*g*) CCDC 2490232: Experimental Crystal Structure Determination, 2026, DOI: 10.5517/ccdc.csd.cc2pl92p; (*h*) CCDC 2490233: Experimental Crystal Structure Determination, 2026, DOI: 10.5517/ccdc.csd.cc2pl93q; (*i*) CCDC 2490234: Experimental Crystal Structure Determination, 2026, DOI: 10.5517/ccdc.csd.cc2pl94r.